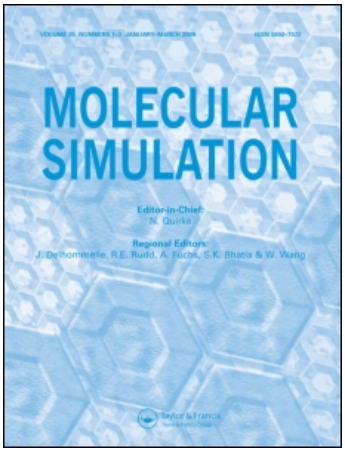

Molecular Simulation
Publication details, including instructions for authors and subscription information:
http://www.informaworld.com/smpp/title~content=t713644482

Density functional computations of Rh(I)-catalysed hydroacylation of acetic aldehyde and ethene

Fen Wang[a]; Qingxi Meng[b]; Ming Li[c]
[a] Department of Chemistry, Taishan University, Taian, Shandong [b] Department of Chemistry and Material Science, Shandong Agricultural University, Taian, Shandong [c] Department of Chemistry, Southwest-China University, Chongqing, P. R. China

To cite this Article Wang, Fen , Meng, Qingxi and Li, Ming(2008) 'Density functional computations of Rh(I)-catalysed hydroacylation of acetic aldehyde and ethene', Molecular Simulation, 34: 5, 515 — 523
To link to this Article: DOI: 10.1080/08927020701753635
URL: http://dx.doi.org/10.1080/08927020701753635

Molecular Simulation
Vol. 34, No. 5, April 2008, 515–523

Taylor & Francis
Taylor & Francis Group

Density functional computations of Rh(I)-catalysed hydroacylation of acetic aldehyde and ethene

Fen Wang[a], Qingxi Meng[b]* and Ming Li[c]

[a]*Department of Chemistry, Taishan University, Taian, Shandong;* [b]*Department of Chemistry and Material Science, Shandong Agricultural University, Taian, Shandong;* [c]*Department of Chemistry, Southwest-China University, Chongqing, P. R. China*

(*Received 21 May 2007; final version received 17 October 2007*)

Density functional theory has been used to study Rh(I)-catalysed hydroacylation of acetic aldehyde and ethene. All the intermediates and the transition states were optimised completely at the B3LYP/6-311 + + G(d,p) level (LANL2DZ(d) for Rh, P). Calculation results confirm that Rh(I)-catalysed hydroacylation of acetic aldehyde and ethene is endothermic, and the total absorbed energy is about 47 kJ/mol. The hydroacylation involves four possible reaction channels, going mainly through Rh–ethene–aldehyde complexes, Rh–ethene–carbonyl complexes, Rh-ethanyl-carbonyl complexes, and Rh-ketone complexes. The formation of Rh–ethene–carbonyl complexes (i.e. Rh(I)-catalysed oxidative addition of aldehyde) is the rate-determinating step for the Rh(I)-catalysed hydroacylation. And the energy barriers of the H-transfer reaction are lower than those of the C–C bond-forming reaction, and thus the H-transfer reaction is prior to the C–C bond-forming reaction. Therefore, the dominant reaction channels predicted theoretically are the reaction channels "a" and "b", which is well in agreement with the experiments.

Keywords: Rh-catalysed hydroacylation; acetic aldehyde; ethene; reaction mechanism; DFT

1. Introduction

Transition metal-catalysed C—H bond activation has received considerable attention in synthetic organic chemistry since the cleavage of an unreactive C—H bond and subsequent addition of the C—H unit into unsaturated substrates such as alkene and alkyne could lead to the formation of a new C—C bond [1–7]. The formation of C—C bond is one of the most fundamental projects in organic chemistry. Much effort has naturally been devoted to develop more convenient and efficient strategies for the formation of C—C bonds. During the last two decades, many successful applications of catalytic C—H bond activation directed toward the construction of C—C bonds have been reported in synthetic communities [8]. The C—C bond-forming reactions via C—H bond activation have extensively been the focus of study in the fields of organic and organometallic chemistry [7–10].

The Rh(I)-catalysed intramolecular and intermolecular hydroacylation (Scheme 1) of alkene or alkyne is one of the most useful C—H bond activation processes [11–20]. The theoretical data available for the mechanism of Rh(I)-catalysed hydroacylation are rather limited. The detailed quantum chemical studies on the mechanism of Rh(I)-catalysed hydroacylation are hardly reported. Therefore, in order to understand the reaction mechanism of Rh(I)-catalysed hydroacylation in detail, Rh(I)-catalysed hydroacylation of acetic aldehyde and ethene is studied in the present work.

2. Models and computations

The present studies are based on Rh(I)-catalysed hydroacylation of acetic aldehyde and ethene [12–16,18–19]. (Scheme 1) As shown in Scheme 2 and Scheme 3, Rh(I)-catalysed hydroacylation of acetic aldehyde and ethene goes mainly through Rh–ethene–aldehyde complexes, Rh–ethene–carbonyl complexes, Rh-ethanyl-carbonyl complexes, and Rh-ketone complexes. Figure 1 shows that Rh–ethene–aldehyde complexes **M1** have two types of geometries which is marked by "a" and "b", respectively. As shown in Figure 1, in **M2a,** the attack of H(6) on C(2) is marked by "a", while the attack of C(5) on C(2) is marked by "c"; in **M2b**, the attack of H(6) on C(2) is marked by "b", while the attack of C(5) on C(2) is marked by "d".

All intermediates and transition states are fully optimised by means of the density functional theory (DFT) [21], with Becke's three-parameter functional (B3) [22] and Lee, Yang, and Parr (LYP) correlation energies [23,24]. The basis set 6-311 + + G(d,p) is for C, O, and H, and LANL2DZ is for Rh and P by adding one set of f-polarisation to rhodium (exponent: 1.350) [25] and one set of d-polarisation to phosphorus (exponent: 0.371) [26]. The vibrational analysis and the natural bond orbital (NBO) analysis [27–34] are performed at the same computational level on the basis of the optimised geometries. All the species are positively identified for local minima with zero of the number of imaginary

*Corresponding author. Email: qingxim@sdau.edu.cn

ISSN 0892-7022 print/ISSN 1029-0435 online

DOI: 10.1080/08927020701753635
http://www.informaworld.com

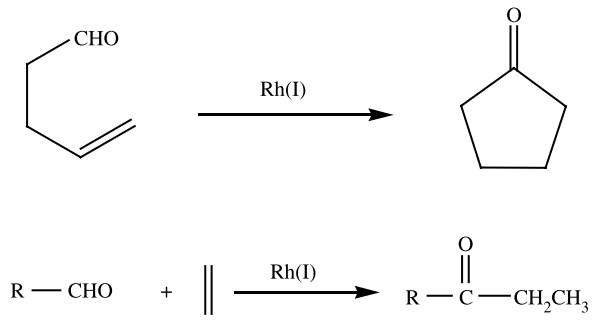

Scheme 1. Intramolecular and intermolecular hydroacylation.

frequencies and for transition states with the sole imaginary frequency. All these computations are carried out by use of the Gaussian 03 program package [35]. Total electronic energies corrected with zero-point energies (ZPE), E, formation energies, ΔE, reaction energy barriers, $\Delta E^{\neq}$, and total Gibbs free energies corrected with ZPE, G, formation Gibbs free energies, ΔG, reaction Gibbs free energy barriers, $\Delta G^{\neq}$, and the first two vibrational frequencies, ν_1 and ν_2, are summarised in Table 1.

The topological properties of the electronic charge density have been characterised using the atoms in molecules (AIM) [36] method of Bader with the AIM 2000 program package. [37]

3. Results and discussion

3.1 Formation of Rh–ethene–carbonyl complexes M2

The optimised structure of the catalyst $Rh(PH_3)_2(CH_2{=}CH_2)_2$ is shown in Figure 2. The Rh(I)-complex ML_4 is square-planar structure, and Rh—P and Rh—C bonds are about 2.35 and 2.31 Å. As illustrated in the NBO analysis, there is the back-donation π bond between rhodium and π bond of ethene. The occupied π orbital of ethene acts on the empty hybrid orbital of rhodium leading to the σ coordinate bond, on the other hand, the occupied d orbital (d_{xy}, d_{xz}, d_{yz}) of rhodium acts on the empty π^* orbital of ethene leading to the back-donation π bond. Obviously, the formation of the back-donation π bonds lowers the system's energy and makes the catalyst more stable.

As shown in Scheme 2, the acetic aldehyde substituting for an ethene leads to the Rh–ethene–aldehyde complexes **M1a** and **M1b**. The transfer of H(6) from C(5) to Rh(3) in the complexes **M1a** and **M1b** leads, via the transition states **TS1a** and **TS1b**, to Rh–ethene–carbonyl complexes **M2a** and **M2b**. This reaction step is generally named as the oxidative addition of aldehyde.

The Rh(I)-complexes **M1** are similar to the catalyst in geometry and all are planar structures, and Rh(3)—O(4) bonds are about 2.19 Å. In the transition states **TS1a** and **TS1b**, as illustrated in Figure 2, C(5)—H(6) bonds are lengthened considerably and Rh(3)—H(6) bonds are shortened, compared with the complexes **M1**. It is clear that there is the significant interaction between Rh(3) and H(6), and the C(5)—H(6) bonds are weakened greatly, which is demonstrated by analysing the changes of the electron densities of the bond critical points (BCPs) (e.g., Rh(3)—H(6) bond, **M1a**: 0.000 → **TS1a**: 0.121 → **M2a**: 0.163). It is demonstrated by the present computations that the fracture of C(5)—H(6) bond and the formation of Rh(3)—H(6) bond may be in concurrence. The complexes **M2a** and **M2b** are pentahedron structure, and the four ligands (ethene, carbonyl, and two groups PH_3) are almost

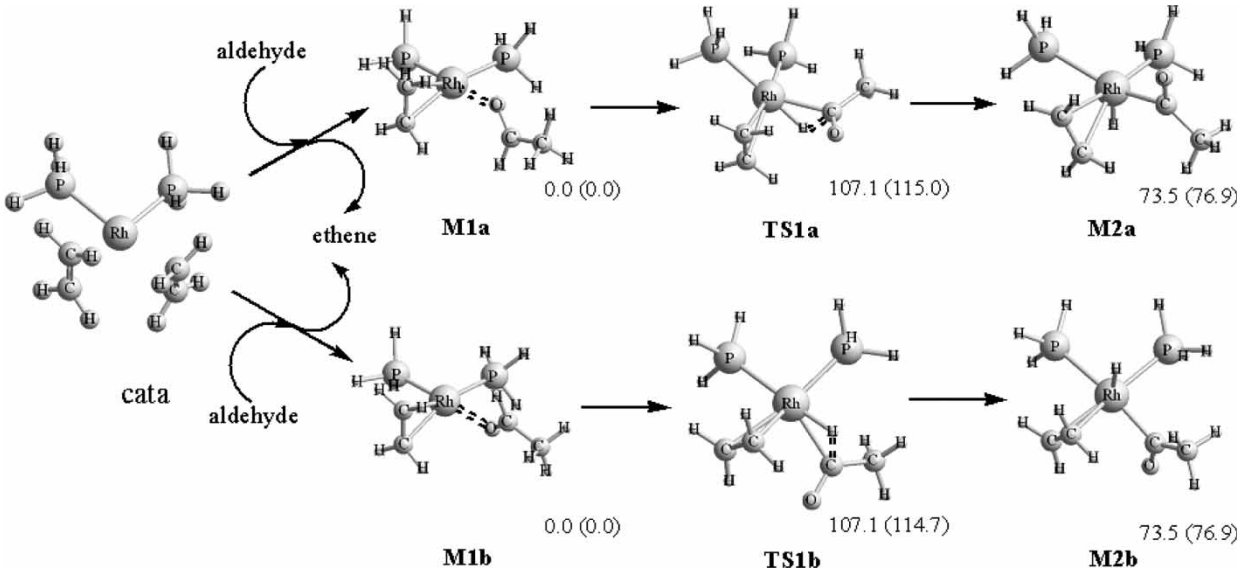

Scheme 2. The formation of the complexes **M2a** and **M2b**. The relative energies are shown in kJ/mol, and in parentheses are relative Gibbs free energies in kJ/mol.

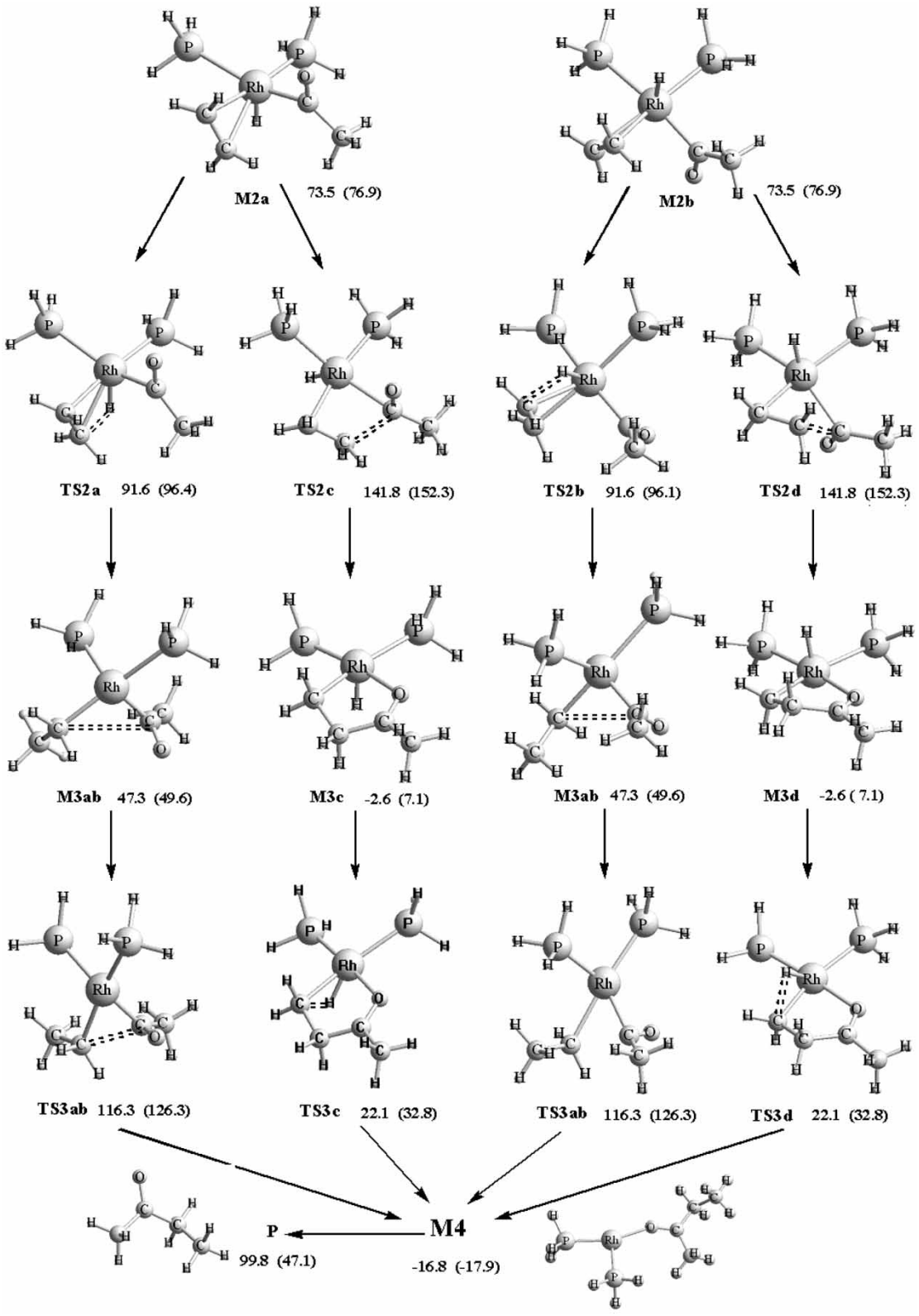

Scheme 3. Reaction channels "**a**", "**b**", "**c**", and "**d**". The relative energies are shown in kJ/mol, and in parentheses are relative Gibbs free energies in kJ/mol.

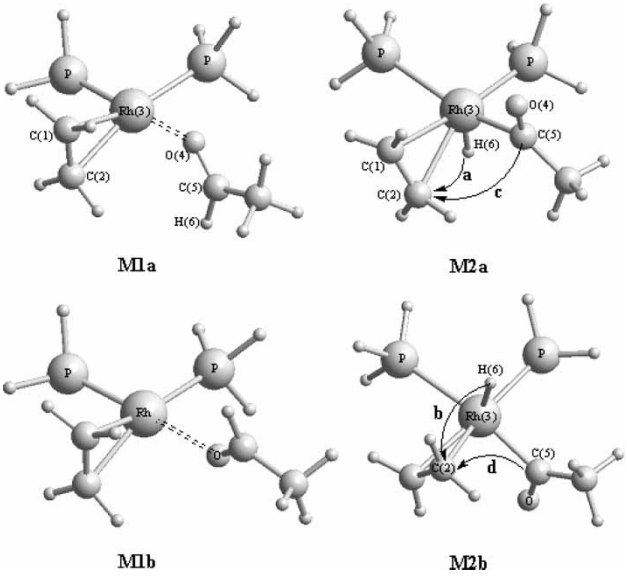

Figure 1. Two types of **M1**, and these four reaction channels in **M2a** and **M2b**.

in a plane and the torsion angles P—P—Rh—C(5) and P—P—Rh—H(6) are about 170° and 80°. There are also the back-donation π bonds between rhodium and π bond of ethene in the complexes **M2a** and **M2b**. As illustrated in the NBO analysis, the Rh(3)—H(6) bonds show strong single-bonded character, the natural bond orbital energies are about − 1250 kJ/mol. And Rh(3)—H(6) bonds are composed of 56% sd^2 hybrid orbital of rhodium and 44% s orbital of hydrogen.

3.2 *Reaction channels "a" and "b"*

3.2.1 *H-transfer*

As shown in Scheme 3, the transfer of H(6) from Rh(3) to C(2) in the complexes **M2a** and **M2b** traverses the transition states **TS2a** and **TS2b**, respectively, and then leads to the Rh–ethanyl–carbonyl complex **M3ab**.

In the transition states **TS2a** and **TS2b**, as illustrated in Figure 2, Rh(3)—H(6) bonds are lengthened considerably and C(2)—H(6) bonds are shortened, compared with the complexes **M2**. These results imply that there is a significant interaction between C(2) and H(6), and the Rh(3)—H(6) bonds are weakened greatly, which is demonstrated by analysing the changes of the electron densities of the BCPs (e.g., Rh(3)—H(6) bond, **M2a**: 0.163 → **TS2a**: 0.133 → **M3ab**: 0.000). It is demonstrated by the present computations that the fracture of Rh(3)—H(6) bond and the formation of C(2)—H(6) bond may be in concurrence. The NBO analysis illustrates that Rh(3)—C(1) bonds show strong single-bonded character, and the natural bond orbital energies are about − 1050 kJ/mol. The transition states **TS2a** and **TS2b** involve a Rh(3)—H(6)—C(2)—C(1) four-membered ring and the electron densities of the ring critical points (RCPs) are 0.0691 and 0.0690, respectively. The Rh–ethanyl–carbonyl complex **M3ab** is of anamorphic tetrahedral

Table 1. Total energies E (× 2625.5 kJ/mol), formation energies $\geq E$ (kJ/mol), reaction energy barriers $\geq E^{\neq}$(kJ/mol), and total Gibbs free energies G (× 2625.5 kJ/mol), formation Gibbs free energies ΔG (kJ/mol), reaction Gibbs free energy barriers $\Delta G^{\neq}$(kJ/mol), and frequencies (cm^{-1}) for all the compounds.

	ZPE	E	≥E	≥E≠	G	≥G	≥G≠	υ1	υ2
cata	0.1628	− 283.0620			− 283.1023			51.18	62.51
re	0.0552	− 153.8271			− 153.8520			153.16	509.83
M1a	0.1659	− 358.3337			− 358.3790			31.08	36.91
M1b	0.1659	− 358.3337			− 358.3790			31.16	37.11
TS1a	0.1624	− 358.2929		107.16	− 358.3352		114.86	432.40i	40.52
TS1b	0.1624	− 358.2929		107.12	− 358.3353		114.74	433.74i	40.17
M2a	0.1625	− 358.3057	− 33.69		− 358.3497	− 37.90		43.49	58.75
M2b	0.1625	− 358.3057	− 33.65		− 358.3497	− 37.82		43.31	58.52
TS2a	0.1609	− 358.2988		18.14	− 358.3423		19.24	630.28i	47.17
TS2b	0.1609	− 358.2988		18.15	− 358.3424		19.23	630.37i	46.07
TS2c	0.1630	− 358.2797		68.26	− 358.3210		75.35	359.12i	59.25
TS2d	0.1630	− 358.2797		68.26	− 358.3210		75.35	356.15i	59.24
M3ab	0.1655	− 358.3157	− 44.28		− 358.3601	− 46.73		30.80	51.37
M3c	0.1654	− 358.3347	− 74.30		− 358.3763	− 69.84		42.81	69.39
M3d	0.1654	− 358.3347	− 76.14		− 358.3763	− 69.84		42.73	69.36
TS3ab	0.1661	− 358.2894		68.96	− 358.3309		76.74	327.18i	63.99
TS3c	0.1646	− 358.3253		24.68	− 358.3665		25.73	777.84i	59.34
TS3d	0.1646	− 358.3253		24.68	− 358.3665		25.73	777.82i	59.35
M4	0.1691	− 358.3401			− 358.3858			22.11	35.05
			− 14.18			− 24.94			
P	0.1123	− 232.4289			− 232.4589			60.79	128.95
ca-2	0.0550	− 125.8574			− 125.8912			16.98	63.49
ethene	0.0508	− 78.5648			− 78.5863			834.91	973.68

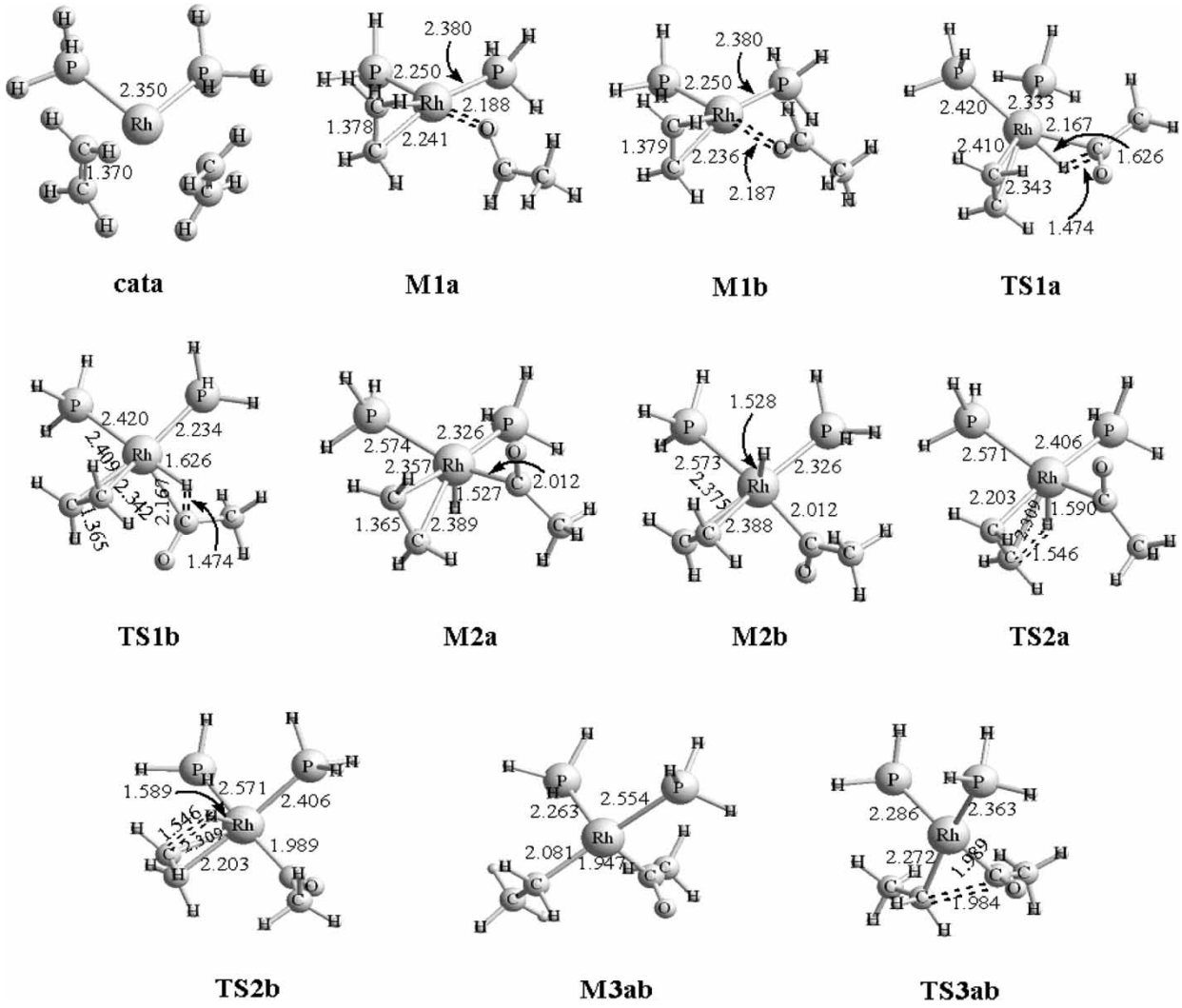

Figure 2. The intermediates and transition states of reaction channels "**a**" and "**b**".

structure, and the C(1)—Rh(3)—C(5)—P torsion angle is 89.8°. As illustrated in the NBO analysis, the Rh(3)—C(1) bonds show strong single-bonded character, and the natural bond orbital energies are about − 1310 kJ/mol. Obviously, Rh(3)—C(1) bonds are strengthened, compared with those of **TS2**. And Rh(3)—C(1) bonds are composed of 50% sd^2 hybrid orbital of rhodium and 50% p orbital of carbon.

3.2.2 *C—C bond-forming reaction*

As shown in Scheme 3, in the complex **M3ab**, the attack of C(1) on C(5) leads, via the transition state **TS3ab**, to the Rh-ketone complex **M4**. The decomposition of the complex **M4** results in the product ketone. In the transition state **TS3ab**, as illustrated in Figure 2, C(1)—C(5) bonds are shortened, compared with the complex **M3ab**. These results imply that there is a significant interaction between C(1) and C(5), which is demonstrated by analysing the changes of the electron densities of the BCPs (e.g., C(1)—C(5) bond, **M3ab**: 0.000 → **TS3ab**: 0.095 → **M4**: 0.261).

3.3 *Reaction channels "c" and "d"*

3.3.1 *C—C bond-forming reaction*

As shown in Scheme 3, in the complexes **M2a** and **M2b**, the attack of C(2) on C(5) leads, via the transition states **TS2c** and **TS2d**, to the complexes **M3c** and **M3d**. In the transition states **TS2c** and **TS2d**, as illustrated in Figure 3, C(2)—C(5) bonds are shortened, compared with the complexes **M3**. These results imply that there is a significant interaction between C(2) and C(5), which is demonstrated by analysing the changes of the electron densities of the BCPs (e.g., C(2)—C(5) bond, **M2c**: 0.000 → **TS2c**: 0.111 → **M3c**: 0.265). The NBO analysis illustrates that Rh(3)—C(1) bonds show strong single-bonded character, and the natural

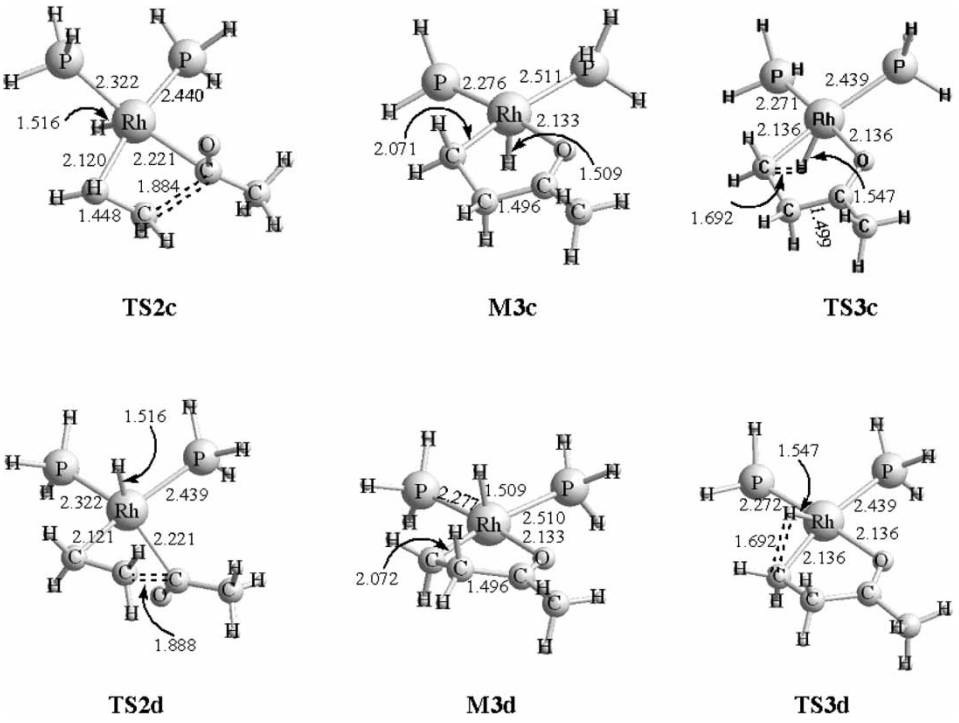

Figure 3. The intermediates and transition states of reaction channels "**c**" and "**d**".

bond orbital energies are about −1140 kJ/mol. And Rh(3)—C(1) bonds are composed of 54% sd^3 hybrid orbital of rhodium and 46% p orbital of carbon. The transition states **TS2c** and **TS2d** involve a Rh(3)—C(5)—C(2)—C(1) four-membered ring and the electron densities of the RCPs are 0.0602. The complexes **M3c** and **M3d** is pentahedron structure, and involve a Rh(3)—C(1)—C(2)—C(5)—O(4) five-membered ring and the electron densities of the RCPs are 0.0257. As illustrated in the NBO analysis, the Rh(3)—C(1) bonds show strong single-bonded character, and the natural bond orbital energies are about −1280 kJ/mol, which is similar to those of the complexes **M3a** and **M3b**. And Rh(3)—C(1) bonds are composed of 46% sd^2 hybrid orbital of rhodium and 54% p orbital of carbon.

3.3.2 *H-transfer*

As shown in Scheme 3, the transfer of H(6) from Rh(3) to C(1) in the complexes **M3c** and **M3d** traverses the transition states **TS3c** and **TS3d**, respectively, and then leads to the complex **M4**. The decomposition of the complex **M4** results in the product ketone. In the transition states **TS3c** and **TS3d**, as illustrated in Figure 3, Rh(3)—H(6) bonds are lengthened considerably and C(1)—H(6) bonds are shortened, compared with the complexes **M3c** and **M3d**. These results imply that there is a significant interaction between C(1) and H(6), and the Rh(3)—H(6) bonds are weakened greatly, which is demonstrated by analysing the changes of electron densities of the BCPs (e.g., Rh(3)—H(6) bond, **M3c**: 0.171 → **TS3c**: 0.168 → **M4**: 0.000). It is demonstrated by the results that formation of C(1)—H(6) bond and the fracture of Rh(3)—H(6) bond may be in concurrence. Being similar to the complexes **M3c** and **M3d**, the transition states **TS3c** and **TS3d** also involve a Rh(3)—C(1)—C(2)—C(5)—O(4) five-membered ring and the electron densities of the RCPs are 0.0602.

3.4 *Stabilisation interaction energies*

The second-order perturbation stabilisation energies *E(2)* obtained by the NBO analysis are summarised in Table 2. It can be used to describe the delocalisation trend of electrons from the donor bond to the acceptor bond. In NBO analysis, if the stabilisation interaction energy *E(2)* between a donor bonding orbital and an acceptor bonding orbital is large, there is a strong interaction between the two bonds.

As demonstrated in Table 2, in **TS1**, there is a strong donor–acceptor interaction between the σ orbital of C(5)—H(6) bond and the LP*(5) orbital of rhodium, which confirm that the electrons in the σ orbital of C(5)—H(6) bond are easy to transfer to the LP*(5) orbital of rhodium.

As presented in Table 3, in **TS2a** and **TS2b**, there is a strong donor–acceptor interaction between the σ orbital of Rh(3)—H(6) bond and the LP*(1) orbital of C(2). These confirm that the electrons in the σ orbital of Rh(3)—H(6)

Table 2. Selected stabilisation interaction energies $E(2)$ for the transition states **TS1**, **TS2**, and **TS3** (kJ/mol).

donor NBO → acceptor NBO	**TS1a**	**TS1b**	**donor NBO → acceptor NBO**	**TS2a**	**TS2b**
LP(3) Rh3 → π* C1—C2	81.7	81.8	LP(1) P → σ* Rh3—C1	393.8	393.8
LP(4) Rh3 → σ* C5—H6	106.5	106.2	σ Rh3—C1 → LP*(1) C2	870.9	870.8
LP(4) Rh3 → π* C5—O4	42.5	42.6	σ Rh3—C1 → σ*Rh3 —C5	328.6	328.5
π C1—C2 → LP*(5) Rh3	74.4	74.7	σ Rh3—C1 → σ*Rh3 —H6	232.7	232.6
π C1—C2 → σ* Rh3—P	223.8	224.1	σ Rh3—H6 → LP*(1) C2	1686.0	1682.5
σ C5—H6 → LP*(5) Rh3	433.8	433.1	σ Rh3—H6 → σ* Rh3—C1	248.1	248.2
			σ Rh3—H6 → σ*Rh3 —C5	359.0	359.1
donor NBO → acceptor NBO	**TS2c**	**TS2d**	**donor NBO → acceptor NBO**	**TS3c**	**TS3d**
LP(1) P → σ* Rh3—C1	514.4	514.4	σ Rh3—P → σ* Rh3—C1	80.2	80.0
σ Rh3—C1 → σ* Rh3—P	321.1	321.1	σ Rh3—P → LP*(1) H6	81.7	81.7
σ Rh3—C1 → σ* Rh3—H6	295.8	295.8	σ Rh3—C1 → σ* Rh3—P	265.1	265.1
σ Rh3—H6 → σ* Rh3—C1	111.7	111.8	σ Rh3—C1 → LP*(1) H6	1298.8	1298.8
σ Rh3—H6 → σ* Rh3—P	198.1	198.1	LP(4) Rh3 → σ* Rh3—P	89.7	89.7
σ Rh3—P → σ* Rh3—H6	160.8	160.8	LP(4) Rh3 → LP*(1) H6	978.5	978.5
σ C2—C5 → σ* Rh3—P	149.4	149.4	LP(2) O4 → σ* Rh3—P	234.2	234.1
LP(2) O4 → σ* C2—C5	161.4	161.4	LP(1) P → σ* Rh3—C1	465.3	465.3
donor NBO → acceptor NBO	**TS3ab**				
LP(4) Rh3 → σ* C1—C5	113.7				
LP(4) Rh3 → π* O4—C5	156.1				
σ C1—C5 → σ* Rh3—P	244.2				
LP(2) O4 → σ* C1—C5	176.0				

bond are easy to transfer to the LP*(1) orbital of C(2), which helps to the fracture of Rh(3)—H(6) bond and the formation of C(2)—H(6) bond. In **TS2c** and **TS2d**, the electrons in the lone pair orbital of phosphorus are easy to transfer to the σ* orbital of Rh(3)—C(1) bond, and the electrons in the σ orbital of Rh(3)—C(1) bond are easy to transfer to the σ* orbitals of Rh(3)—P bond and Rh(3)—H(6) bond, which makes **TS2c** and **TS2d** more stable. In **TS3c** and **TS3d**, there is a strong donor–acceptor interaction between the σ orbital of Rh(3)—C(1) bond and the LP*(1) orbital of H(6). These confirm that the electrons in the σ orbital of Rh(3)—C(1) bond are easy to transfer to the LP*(1) orbital of H(6), which helps to the fracture of Rh(3)—C(1) bond and the formation of C(1)—H(6) bond.

3.5 Overview of the mechanism

As discussed above, Rh(I)-catalysed hydroacylation of acetic aldehyde and ethene goes mainly through Rh–ethene–aldehyde complexes, Rh–ethene–carbonyl complexes, Rh–ethanyl–carbonyl complexes, and Rh–ketone complexes. As shown in Schemes 2 and 3, the reaction goes mainly through the transition states **TS1**, **TS2**, and **TS3**. Figure 4 illustrates the DFT free energy profiles for Rh(I)-catalysed hydroacylation of aldehyde and ethane.

Table 1 show that the formation of the complexes **M2**, **M3**, and **M4** are exothermic. Rh(I)-catalysed hydroacylation of acetic aldehyde and ethene is endothermic, and the total absorbed energy is about 47 kJ/mol.

As shown in Table 1, the energy barriers of the transition states **TS1a** and **TS1b** are about 115 kJ/mol. The energy barriers of the transition states **TS2a**, **TS2b**, **TS2c**, and **TS2d** are 19, 19, 75, and 75 kJ/mol, respectively. The energy barriers of the transition states **TS3ab**, **TS3c**, and **TS3d** are 76, 26, and 26 kJ/mol, respectively. Obviously, the energy barriers of the transition states **TS1** are higher than those of the transition states **TS2** and **TS3**. Therefore, the formation of Rh–ethene–carbonyl complexes **M2** (i.e. Rh(I)-catalysed oxidative addition of aldehyde) is the rate-determinating step for the Rh(I)-catalysed hydroacylation. In the reaction channels "a" and "b", the energy barriers of the transition states **TS2a** and **TS2b** are lower than those of the transition state **TS3ab**. But in the reaction channels "c" and "d", the

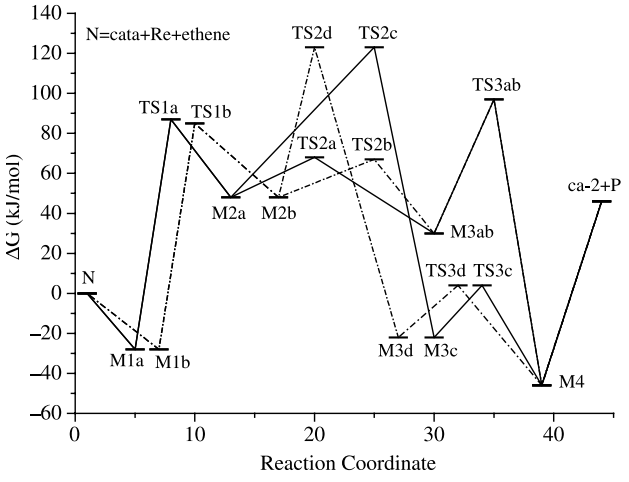

Figure 4. Free energy relationship for Rh(I)-catalysed hydroacylation of aldehyde and ethene.

energy barriers of the transition states **TS2c** and **TS2d** are higher than those of the transition states **TS3c** and **TS3d**. So the energy barriers of the H-transfer reaction are lower than those of the C—C bond-forming reaction, and thus the H-transfer reaction is prior to the C—C bond-forming reaction. Accordingly, the dominant reaction channels of Rh-catalysed hydoacylation are the reaction channels "a" and "b": **M1a → TS1a → M2a → TS2a → M3ab → → TS1a → M2a → TS2a → M3ab → TS3ab → M4 → → M3ab → TS3ab → M4 → P** and **M1b → TS1b → M2b → TS2b → M3ab → TS3ab → M4 → P**, which is well agreement with these experiments [12–15].

4. Conclusion

In summary, Rh(I)-catalysed hydroacylation of acetic aldehyde and ethene involves four possible reaction channels, going mainly through Rh–ethene–aldehyde complexes, Rh–ethene–carbonyl complexes, Rh–ethanyl–carbonyl complexes, and Rh–ketone complexes. Calculation results confirm that Rh(I)-catalysed hydroacylation is endothermic, and the total absorbed energy is about 47 kJ/mol. The formation of Rh–ethene–carbonyl complexes (i.e. Rh(I)-catalysed oxidative addition of aldehyde) is the rate-determinating step for the Rh(I)-catalysed hydroacylation. And the energy barriers of the H-transfer reaction are lower than those of the C—C bond-forming reaction, and thus the H-transfer reaction is prior to the C—C bond-forming reaction. Therefore, the dominant reaction channels predicted theoretically are the reaction channels "a" and "b", which is well agreement with these experiments.

References

[1] C. Jun and J.H. Lee, *Application of C—H and C—C bond activation in organic synthesis*, Pure. Appl. Chem. 76 (2004), p. 577.

[2] C. Jia, T. Kitamura, and Y. Fujiwara, *Catalytic functionalization of arenes and alkanes via C—H bond activation*, Acc. Chem. Res. 34 (2001), p. 633.

[3] F. Kakiuchi and S. Murai, *Activation of C—H bonds: catalytic reactions*, Top. Organomet. Chem. 3 (1999), p. 47.

[4] Y. Guari, S. Sabo-Etienne, and B. Chaudret, *Catalytic formation of carbon–carbon bonds by activation of carbon–hydrogen bonds*, Eur. J. Inorg. Chem. 1999 (1999), p. 1047.

[5] B.A. Arndtsen, R.G. Bergman, A. Mobley, and T.H. Peterson, *Selective intermolecular carbon–hydrogen bond activation by synthetic metal complexes in homogeneous solution*, Acc. Chem. Res. 28 (1995), p. 154.

[6] A.E. Shilov and G.B. Shul′pin, *Activation of C—H bonds by metal complexes*, Chem. Rev. 97 (1997), p. 2879.

[7] G. Dyker, *Transition metal catalyzed coupling reactions under C—H activation*, Angew. Chem. Int. Ed. 38 (1999), p. 1698.

[8] V. Ritleng, C. Sirlin, and M. Pfeffer, Ru-, Rh-, and Pd-catalyzed C—C bond formation involving C—H activation and addition on unsaturated substrates: reactions and mechanistic aspects, Chem. Rev. 102 (2002), p. 1731.

[9] J.A. Labinger and J.E. Bercaw, *Understanding and exploiting C—H bond activation*, Nature 417 (2002), p. 507.

[10] F. Kakiuchi and S. Murai, *Catalytic C—H/Olefin coupling*, Acc. Chem. Res. 35 (2002), p. 826.

[11] S.-I. Inoue, H. Takaya, K. Tani, S. Otsuka, T. Sato, and R. Noyori, *Mechanism of the asymmetric isomerization of allylamines to enamines catalyzed by 2,2′-bis(diphenylphosphino)-1,1′binaphthyl-rhodium complexes*, J. Am. Chem. Soc. 112 (1990), p. 4897.

[12] S.H. Bergens and B. Bosnich, *Homogeneous catalysis*, Catalytic production of simple enols, J. Am. Chem. Soc. 113 (1991), p. 958.

[13] R.W. Barnhart, X.-Q. Wang, P. Noheda, S.H. Bergens, J. Whelan, and B. Bosnich, *Asymmetric catalysis. Asymmetric catalytic intramolecular hydroacylation of 4-pentenals using chiral Rhodium diphosphine catalysts*, J. Am. Chem. Soc. 116 (1994), p. 1821.

[14] C.-H. Jun, J.-B. Hong, and D.-Y. Lee, *Chelation-assisted hydroacylation*, Synlett (1999), p. 1.

[15] A.D. Aloise, M.E. Layton, and M.D. Shair, *Synthesis of cyclooctenones using intramolecular hydroacylation*, J. Am. Chem. Soc. 122 (2000), p. 12610.

[16] C.-H. Jun, J.-H. Chung, D.-Y. Lee, A. Loupy, and S. Chatti, *Solvent-free chelation-assisted intermolecular hydroacylation: effect of microwave irradiation in the synthesis of ketone from aldehyde and 1-alkene by Rh(I) complex*, Tetrahedron Lett. 42 (2001), p. 4803.

[17] K. Tanaka and G.C. Fu, *A Versatile new method for the synthesis of cyclopentenones via an unusual rhodium-catalyzed intramolecular trans hydroacylation of an alkyne*, J. Am. Chem. Soc. 123 (2001), p. 11492.

[18] M.C. Willis and S. Sapmaz, *Intermolecular hydroacylation of acrylate esters: a new route to 1,4-dicarbonyls*, Chem. Commun. (2001), p. 2558.

[19] C.-H. Jun, C.W. Moon, and D.-Y. Lee, *Chelation-assisted carbon–hydrogen and carbon–carbon bond activation by transition metal catalysts*, Chem. Eur. J 8 (2002), p. 2423.

[20] K. Tanaka, and G.C. Fu, *Parallel kinetic resolution of 4-alkynals catalyzed by Rh(I)/Tol-BINAP: synthesis of enantioenriched cyclobutanones and cyclopentenones*, J. Am. Chem. Soc. 125 (2003), p. 8078.

[21] R.G. Parr and W. Yang, *Density-functional Theory of Atoms and Molecules*, Oxford University Press, New York, 1989.

[22] A.D. Becke, *Density-functional thermochemistry. III. The role of exact exchange*, J. Chem. Phys. 98 (1993), p. 5648.

[23] C. Lee, W. Yang, and R.G. Parr, *Development of the Colle–Salvetti correlation-energy formula into a functional of the electron density*, Phys. Rev. B 37 (1988), p. 785.

[24] B. Miehlich, A. Savin, H. Stoll, and H. Preuss, *Results obtained with the correlation energy density functionals of becke and Lee, Yang and Parr*, Chem. Phys. Lett. 157 (1989), p. 200.

[25] A. Höllwarth, M. Böhme, S. Dapprich, A.W. Ehlers, A. Gobbi, K.F. Köhler, R. Stegmann, A. Veldkamp, and G. Frenking, *A set of d-polarization functions for pseudo-potential basis sets of the main group elements Al–Bi and f-type polarization functions for Zn, Cd, Hg*, Chem. Phys. Lett. 208 (1993), p. 237.

[26] A.W. Ehlers, M. Böhme, S. Dapprich, A. Gobbi, A. Höllwarth, V. Jonas, K.F. Köhler, R. Stegmann, A. Veldkamp, and G. Frenking, *A set of f-polarization functions for pseudo-potential basis sets of the transition metals Sc–Cu, Y–Ag and La–Au, Chem*, Phys. Lett. 208 (1993), p. 111.

[27] E.D. Glendening, A.E. Reed, J.E. Carpenter, and F. Weinhold, NBO Version 3.1

[28] J.E. Carpenter and F. Weinhold, *Analysis of the geometry of the hydroxymethyl radical by the "different hybrids for different spins" natural bond orbital procedure*, J. Mol. Struct. (THEOCHEM) 169 (1988), p. 41.

[29] J.P. Foster and F. Weinhold, *Natural hybrid orbitals*, J. Am. Chem. Soc. 102 (1980), p. 7211.

[30] A.E. Reed and F. Weinhold, *Natural bond orbital analysis of near-Hartree–Fock water dimmer*, J. Chem. Phys. 78 (1983), p. 4066.

[31] ———, *Vibrational–rotational energy transfer in collisions of HF (v = 4, J = 20) with rare gases*, J. Chem. Phys. 78 (1983), p. 1736.

[32] A.E. Reed, R.B. Weinstock, and F. Weinhold, *Natural population analysis*, J. Chem. Phys. 83 (1985), p. 735.

[33] A.E. Reed, L.A. Curtiss, and F. Weinhold, *Intermolecular interactions from a natural bond orbital, donor–acceptor viewpoint*, Chem. Rev. 88 (1988), p. 899.
[34] F. Weinhold and J.E. Carpenter, *The structure of small molecules and ions*, Vol. 227, Plenum, New york, 1988.
[35] M.J. Frisch, G.W. Trucks, H.B. Schlegel, G.E. Scuseria, M.A. Robb, J.R. Cheeseman, J.A. Montgomery, J.T. Vreven, K.N. Kudin, J.C. Burant et al., *Gaussian 03. Revision B.03, Gaussian, Inc., Pittsburgh PA*, 2003.
[36] R.F.W. Bader, *Atoms in Molecules, A Quantum Theory; International Series of Monographs in Chemistry*, Vol. 22, Oxford University Press, Oxford, UK, 1990.
[37] F. Biegler-König, J. Schönbohm, R. Derdau, D. Bayles, and R.F.W. Bader, *AIM 2000. Version 1*, 2000.